JOURNAL OF PROPULSION AND POWER
Vol. 21, No. 2, March–April 2005

Pressure Effects on Flowing Mildly-Cracked n-Decane

Thomas A. Ward,* Jamie S. Ervin,† and Steven Zabarnick‡
University of Dayton, Dayton, Ohio 45469-0210
and
Linda Shafer§
University of Dayton Research Institute, Dayton, Ohio 45469-0116

It is anticipated that traditional methods of cooling that employ the sensible heat transfer provided by fuels will not be sufficient to meet the cooling requirements of future high-performance aircraft. One potential solution is the use of endothermic fuels, which absorb heat through chemical reactions. However, few studies have analyzed the effects of pressure on a chemically reacting, flowing fuel. An experiment is described that studies the effects of pressure on flowing, mildly cracked, supercritical n-decane. The experimental results are studied with the aid of a unique two-dimensional computational fluid dynamics model that simulates the formation of cracked products from experimentally derived proportional distributions. This model is used to study the effect of pressure on the flow properties of the fuel. The experiments indicate that increasing pressure enhances bimolecular pyrolysis reactions, relative to unimolecular reactions. Increasing pressure also increases the overall conversion rate of supercritical n-decane flowing through a reactor. This is primarily because pressure increases the density, which increases the residence time of n–decane flowing through the reactor.

Nomenclature

A	=	preexponential factor (A factor) in Arrhenius rate expression, s^{-1}
C_p	=	specific heat, J/kg · K
C_μ	=	coefficient in turbulent transport equations, const = 0.09
C_1	=	coefficient in turbulent transport equations, const = 1.47
C_2	=	coefficient in turbulent transport equations, const = 1.92
D_i	=	diffusion coefficient of ith species, m^2/s
E_a	=	activation energy in Arrhenius rate expression, cal/mole
G	=	$\mu_t\{2[(\partial u/\partial z)^2 + (\partial v/\partial r)^2 + (v/r)^2] + [(\partial v/\partial z) + (\partial u/\partial r)]^2\}$
g	=	gravitational acceleration, m/s^2
h	=	enthalpy, kJ/kg
h_{sens}	=	enthalpy due to sensible heat transfer, kJ/kg
h_{tot}	=	total enthalpy, kJ/kg
i	=	individual product species
k	=	turbulent kinetic energy, kJ/kg
k_A	=	Arrhenius rate constant, s^{-1}
p	=	pressure, MPa
Q_{endo}	=	heat transfer due to endothermic reactions, W
Q_{sens}	=	sensible heat transfer, W
Q_{tot}	=	total heat transfer, W
R	=	gas constant, 1.987 cal/K · mole
r	=	radial coordinate, (m)
S^Φ	=	source term
T	=	fuel temperature, °C or K
t	=	time, s
u	=	axial velocity component, m/s
v	=	radial velocity component, m/s
Y_i	=	mass fraction of ith cracked product species (fraction includes parent fuel)
Y_{RH}	=	mass fraction of parent fuel
$Y_{\sum \text{products}}$	=	mass fraction of total products
y_i	=	product mass fraction of ith product species (fraction excludes parent fuel)
$y_{i_{\text{av}}}$	=	averaged y_i over a range of parent fuel conversions
z	=	axial coordinate, m
Γ^Φ	=	transport coefficient
Δh_{endo}	=	enthalpy change due to endotherm, kJ/kg
ε	=	turbulence dissipation rate, W
κ	=	thermal conductivity, W/m · K
μ	=	absolute viscosity, kg/m · s
μ_t	=	turbulent viscosity, $C_\mu \cdot \rho \cdot k^2/\varepsilon$, kg/m · s
ρ	=	density, kg/m^3
σ_k	=	effective turbulent Prandtl number (kinetic energy), const = 1.0
σ_{Y_i}	=	effective turbulent Prandtl number (species), const = 1.0
σ_ε	=	effective turbulent Prandtl number (dissipation rate), const = 1.3
Φ	=	assigned variable in Eq. (2)
$\dot{\omega}_i$	=	rate of production of ith species, $kg/m^3 \cdot s$

Received 4 December 2003; revision received 19 July 2004; accepted for publication 2 July 2004.

*Aerospace Engineer, Department of Mechanical and Aerospace Engineering; Thomas.Ward@wpafb.af.mil. Member AIAA.

†Professor, Department of Mechanical and Aerospace Engineering; also Group Leader, Modeling and Simulation. Associate Fellow AIAA.

‡Professor, Department of Mechanical and Aerospace Engineering; also Distinguished Research Chemist, Fuels Science.

§Chemist, Fuels Science Group.

Introduction

IN advanced military jet engines, fuel is used for cooling before combustion. It is envisioned that the heat dissipation requirements of future high-performance aircraft will increase beyond that which can be supplied by the sensible heat transfer provided by fuels.[1] Use of cryogenic fuels would add unacceptable weight, complexity, and cost. An alternative solution is to use a hydrocarbon fuel that absorbs heat through a series of endothermic chemical reactions. With an endothermic fuel, additional cooling is obtained by endothermic reactions occurring simultaneously with traditional convective heat transfer. The endothermic heat absorption rate can be over twice that of rate available by sensible cooling.[1]

Significant thermal cracking of jet fuel occurs at temperatures above approximately 500°C, where the bonds of hydrocarbon molecules are broken to produce several smaller molecules. This type of endothermic reaction is called thermal cracking or

pyrolysis.[2] However, there are numerous factors that must be studied and understood before pyrolysis cooling can be applied to a new heat exchanger design. The effects of fuel temperature and residence time on pyrolytic fuel flow have been popular past topics of study, due to their strong influence on the reaction rate.[3] Unfortunately, there is little work that addresses the effects of pressure on fuel properties and very few computational models capable of sufficiently representing the problem. A change of pressure on a flowing, supercritical hydrocarbon fuel may affect the flow properties. The effect of these properties on the velocity, heat transfer, and chemical kinetics is complex, especially if multidimensional geometries are considered. Furthermore, chemical changes in the fuel as it cracks also affect the behavior of flowing fuel. All of these factors must be taken into account to understand the effect of pressure completely.

Fabuss et al.[4] conducted flow experiments to study the effects of pressure on the thermal cracking of n–hexadecane pumped at different flow rates (16–133 ml/min). The reactor was placed inside a furnace, which heated the reactor to wall temperatures over the range of 600–700°C. Analysis and measurements of the products were done by several methods, including gas chromatography. They concluded that, although the overall conversion of hexadecane increased with increasing pressure, the first-order reaction rate constants for the cracking of hexadecane was independent of pressure over the range studied (1.38–6.89 MPa). Unfortunately, they did not model the experiment or analyze the flow properties.

Similarly, Jones et al.[5] conducted flow experiments using a mixture of n–alkanes (Norpar-13) pumped at a flow rate of 20 ml/min over a pressure range from 3.5–16.3 MPa. The reactor was electrically heated to produce an exit fuel temperature of 635°C. The gaseous products were collected in a bag after the fuel was cooled to room temperature and analyzed using gas chromatography. The liquid products were also analyzed by gas chromatography, but the measurements were lumped in carbon number groupings rather than differentiated as individual product species. Furthermore, a simple calculation of conversion was used and was defined as the fraction of liquid lost in the reaction region (with the final quantity of liquid being determined after cooling to room temperature). This definition of conversion ignores the liquid products and is, therefore, an inaccurate measure of conversion. Whereas they overlooked this inaccuracy due to their focus on deposition, the development of a computational model to study the flow properties of the fuel requires a more accurate definition of conversion that considers the liquid products.

The experiments of the present work study the effect of pressure on flowing n–decane undergoing mild-cracking reactions. Mild cracking is defined as a low conversion of n–decane in which the primary degradation products are smaller carbon number n–alkanes and 1–alkenes.[6–8] Mild-cracking reactions of n–alkanes do not form aromatics in substantial quantities. Aromatics are known to increase soot and pollutant emissions during combustion, reduce the heat-absorbing potential of the reaction, and are thought to be deposition precursors.[9] Deposition is undesirable because it can obstruct fuel pathways, resulting in catastrophic system failure. Therefore, mild-cracking reactions of n–alkanes are of interest in endothermic fuel systems. A single-pass heat exchanger, designed for mild-cracking reactions, could potentially provide a beneficial heat sink with minimal deposition and its associated detrimental effects. Research focused on suppressing surface deposition by use of surface coatings and additives is also ongoing.[10]

In this work, a two-dimensional computational fluid dynamics model is used to assist the understanding of the transport properties of the fuel. Many flow properties of interest in fuel experiments are difficult or costly to measure. Also measuring devices can sometimes interfere with the measurement of a flow property, providing erroneous data or resulting in undesirable conditions. Numerical models aid in understanding endothermic fuel experiments by simulating properties that are unavailable from measurement. Most past pyrolytic modeling efforts have involved several different types of chemical kinetics mechanisms including detailed, lumped, and global. Detailed[11] and lumped[7,12] kinetic mechanisms have generally been confined to nonflowing, analytical models. Detailed modeling of pyrolysis requires knowledge of thousands of elementary reaction pathways and rate constants, which are generally unavailable for high carbon number n–alkanes.[11] Thus, incorporation of a detailed model into multidimensional fluid dynamics problems is generally not practical. Lumped mechanisms group components of a fuel/product mixture into kinetic lumps, which are then treated as pseudocomponents. However, information about individual components comprising the product distribution is lost. Therefore, the transport properties associated with the mixture may not be adequately modeled. Most past numerical simulations of the thermal cracking of flowing jet fuel have employed global kinetic mechanisms.[13–15] In global mechanisms, only the rate equations for the primary fuel species or components are defined. Because global mechanisms generally require fewer rate equations than detailed or lumped mechanisms, they are the most practical mechanisms for multidimensional fluid dynamics applications. However, most global models do not account for property changes due to the formation of cracked products.[13–15]

In a previous study, we developed a new mechanism that calculated mildly cracked products based on experimentally measured proportional distributions.[3] This proportional product distribution (PPD) mechanism is able to simulate chemical composition changes of a fuel as it undergoes pyrolysis. The PPD mechanism requires only one rate expression defining n–decane degradation. In this previous work, we demonstrated the advantages of using the PPD mechanism over a range of temperatures and flow rates, but for only one pressure, 3.45 MPa (Ref. 3). In the current work, we apply the PPD mechanism to a range of pressures to study the effect of pressure on a flowing, mildly cracked fuel.

Experimental

A set of experiments was performed to study the effect of pressure on the products of n–decane pyrolysis (Aldrich 99+%). N–decane was selected because it has a critical pressure and temperature similar to those of actual jet fuels, for example, jet-A and JP-8). Use of a pure compound avoids difficulties in differentiating specific product yields resulting from a complex mixture of reactants comprising an actual jet fuel. Studies have shown that n–alkanes (like n–decane) have product distributions that are similar to real jet fuels for experimental conditions similar to those studied in this work.[16] The experimental apparatus used was the system for thermal diagnostic studies (STDS), shown in Fig. 1. The STDS consists of a thermal reaction chamber, gas chromatograph (GC) with mass spectrometer (MS), and hydrogen flame ionization detectors (FID).

The n–decane was sparged with gaseous helium before being pumped into the STDS to displace dissolved oxygen to prevent thermal-oxidative deposition in the heated reactor. A syringe pump was used to provide a constant flow rate through the reactor, and three different flow rates were used, 0.3, 0.5, 0.7 ml/min. The fuel was pumped into 316 stainless steel tubing (0.5 mm i.d.) and passed through a switch valve that either directed the fuel to the reactor assembly or allowed gaseous nitrogen to flow through the system (to prevent surface deposition in the reactor when not collecting data).

A series of backpressure regulators were used to obtain five different outlet pressures, 3.45, 5.17, 7.93, 9.31, and 11.38 MPa. An in-line pressure gauge was used to verify the pressure settings. The thermal reaction chamber was housed in a GC oven (Hewlett–Packard Model 5890A) kept at 200°C. The oven was used for temperature control of the fuel transfer lines into the reactor. Contained inside this oven was a smaller high-temperature furnace that completely surrounded the reactor and heated it by electrically resistive coils. The heating coils were surrounded by insulation to minimize convective heat loss to the surrounding GC oven. The reactor consisted of a continuous coiled, stainless steel fuel line (1.6 mm o.d. × 0.5 mm i.d. × 34.3 cm in length) lying inside an insulated quartz tube. The quartz tube was capped at both ends with a foam insulator to reduce convective heat loss. Six (type K) thermocouples were strap welded onto the outer wall of the reactor (Fig. 2).

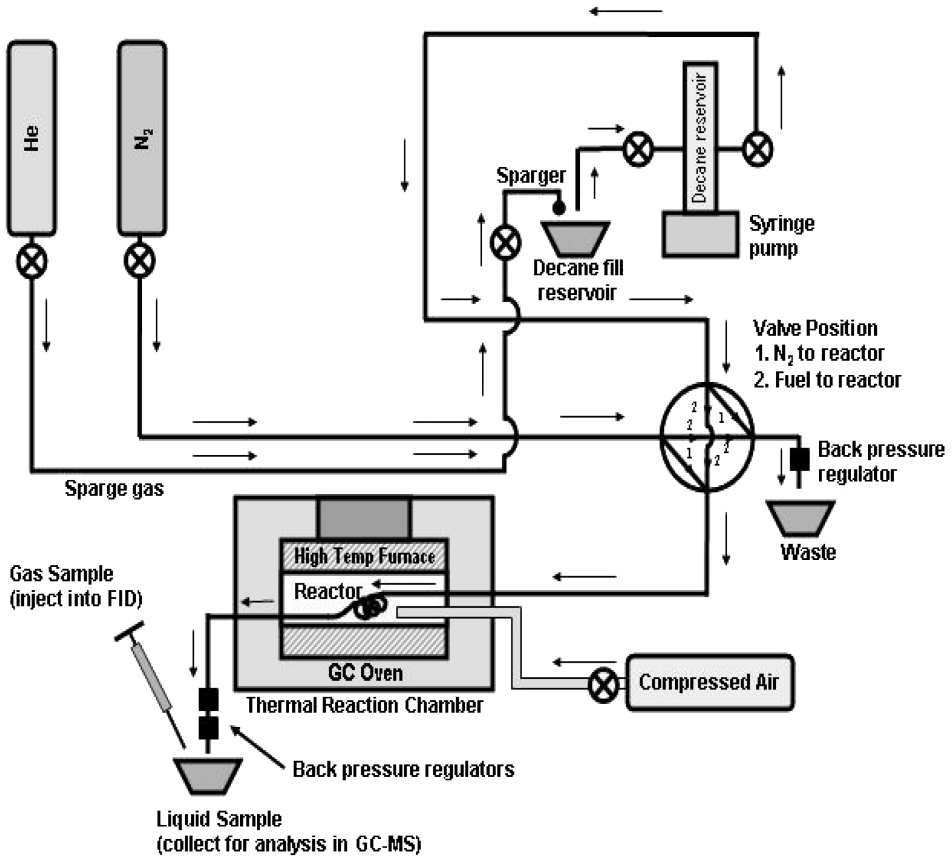

Fig. 1 STDS experimental apparatus.

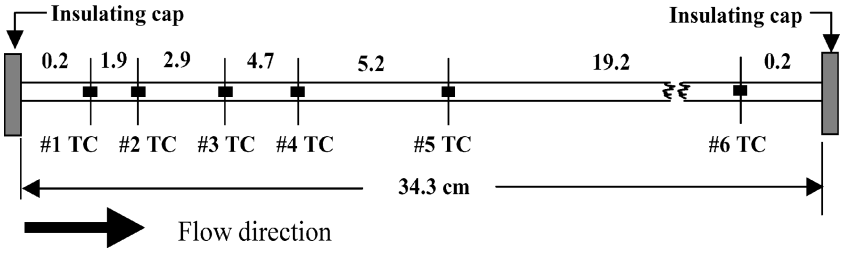

Fig. 2 Flow reactor Schematic, not to scale; all units in centimeters; thermocouples (TC) indicated.

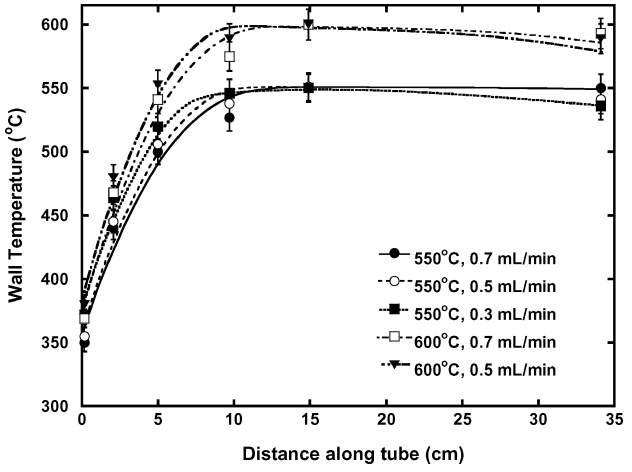

Fig. 3 Measured wall temperatures, 3.45 MPa.

The measured wall temperature profiles (uncertainty of ±2°C) were used as boundary conditions for the numerical model. Two maximum wall temperature profiles were used, which had maximum temperatures of 550 or 600°C measured at the fifth thermocouple. As the fuel cracks, the endothermic reaction cools the fuel and the reactor wall. Because the magnitude of the endotherm varies with the different flow conditions, the electrical power supplied to the high-temperature furnace was adjusted (in response to different conditions) to maintain a constant maximum wall temperature (550 or 600°C) at the fifth thermocouple. Figure 3 shows the wall temperature profiles measured at a pressure of 3.45 MPa. The wall temperatures measured at the other pressure settings were similar to those shown in Fig. 3 and, thus, are not shown. The experiment was run at different flow rates for five pressure conditions and two maximum wall temperatures.

As fuel exited the reactor and cooled to room temperature, gas product samples were collected from a liquid/gas separator in a syringe and then injected into the FID. Ultrahigh purity helium (99.999%) was used as the carrier gas. The condensed-phase (liquid)

Table 1 Source terms and transport coefficients appearing in Eqs. (1) and (2)

Φ	Γ^{Φ}	S^{Φ}
u	$\mu+\mu_t$	$-\frac{\partial p}{\partial z}+\frac{\partial}{\partial z}\left(\Gamma^u\frac{\partial u}{\partial z}\right)+\frac{\partial}{\partial r}\left(\Gamma^u\frac{\partial v}{\partial z}\right)+\frac{\Gamma^u}{r}\frac{\partial v}{\partial z}+\rho g$
v	$\mu+\mu_t$	$-\frac{\partial p}{\partial r}+\frac{\partial}{\partial z}\left(\Gamma^v\frac{\partial u}{\partial r}\right)+\frac{\partial}{\partial r}\left(\Gamma^v\frac{\partial v}{\partial r}\right)+\frac{\Gamma^v}{r}\frac{\partial v}{\partial r}-2\,\Gamma^v\frac{v}{r^2}$
k	$\mu+\mu_t/\sigma_k$	$G-\rho\varepsilon$
ε	$\mu+\mu_t/\sigma_\varepsilon$	$C_1G(\varepsilon/k)-C_{2\rho}(\varepsilon^2/k)$
h	$\kappa/c_p+\mu_t/\sigma_h$	0
Y_i	$\rho D_i+\mu_t/\sigma_{y_i}$	$\dot{\omega}_i$

product samples were collected for 15 min, weighed, and analyzed off-line using a GC–MS (Hewlett–Packard Model 5890A). The mass of the total gas products was determined by subtracting the weight of these liquid samples by a 15-min sample of unreacted n–decane (pumped through the STDS but unheated). The liquid and gas product fractions (determined from the GC–MS and FID, respectively) were normalized with the measured total gas and liquid product masses (for a 15-min sampling time) so that they could be directly related to one another. Once the product fractions were normalized (to the same sampling time), a product distribution including all products (gas and liquid) was calculated.

Both the FID and GC–MS were calibrated with external standards spanning the entire range of products formed in the experiment. All of the product species were quantified based on these calibrations. Six replicates of each experimental condition were performed to obtain an indication of the experimental error. The maximum standard deviation of the measured parent fuel mass fraction from all of the experimental conditions was $\pm 0.8\%$.

Computational Fluid Dynamics Simulations

The computational fluid dynamics (CFD) model is based upon the SIMPLE algorithm, which uses the Navier–Stokes turbulent energy, enthalpy, and species equations to simulate the flow and heat and mass transport within the reactor.[17] The fluid motion inside the reactor was assumed to be axisymmetric and steady. The governing equations written in the cylindrical (z, r) coordinate system for axisymmetric flow are

$$\frac{\partial(\rho u)}{\partial z}+\frac{\partial(\rho v)}{\partial r}+\frac{\rho v}{r}=0 \tag{1}$$

$$\frac{\partial(\rho u\Phi)}{\partial z}+\frac{\partial(\rho v\Phi)}{\partial r}=\frac{\partial}{\partial z}\left(\Gamma^{\Phi}\frac{\partial\Phi}{\partial z}\right)+\frac{\partial}{\partial r}\left(\Gamma^{\Phi}\frac{\partial\Phi}{\partial r}\right)-\frac{\rho v\Phi}{r}+\frac{\Gamma^{\Phi}}{r}\frac{\partial\Phi}{\partial r}+S^{\Phi} \tag{2}$$

Equation (1) is the continuity equation, and Eq. (2) represents the momentum, energy, or species equation depending on the variable represented by Φ. Here, ρ is the mixture density. Table 1 lists the transport coefficients Γ^{Φ} and the source terms S^{Φ} of the governing equations. The governing equations are discretized utilizing a second-order, central differencing scheme (except where the local Peclet number becomes greater than two, in which case a first-order upwind scheme is used). The solution was considered converged when the velocity, pressure, turbulent kinetic energy, turbulent dissipation, enthalpy, and species global error residuals were all reduced below four orders of magnitude from their maximum values.

The inlet velocity and temperature profile of the fuel are assumed to be uniform for simplicity. The inlet fuel temperature was 200°C. A wall temperature profile (obtained from measured data) was input as a boundary condition. Wall functions were used to determine the flow variables near the wall.[18] Because the purpose of the model is to simulate mild thermal cracking, resulting in very low surface deposition, deposition was not modeled.

One of the salient features of the computational model is that it does not use idealized approximations such as plug flow or constant properties. Because endothermic fuels will be expected to operate at supercritical temperatures and pressures, it is important to assess fuel behavior under supercritical conditions. Supercritical behavior occurs when both the temperature and pressure reach or exceed the critical point of the fuel. Supercritical fluids are characterized by having a low, gaslike viscosity and a high, liquidlike density. Transition from liquid phase to supercritical state may strongly influence the transport properties that ultimately determine the effects of pressure on the temperature field, reaction rates, and cooling capacity. The thermodynamic and transport properties were calculated at every grid point by incorporating SUPERTRAPP[19] subroutines. SUPERTRAPP performs phase equilibrium calculations with the Peng–Robinson equation of state,[20] and transport properties are calculated with an extended corresponding states model. SUPERTRAPP provides well-behaved thermodynamic properties near the critical point and in the supercritical regime. However, it does not calculate the molecular diffusivity. Determination of diffusion coefficients for supercritical conditions is difficult, and there is little specific literature on the subject. In a previous work, we showed that the molecular diffusivity has a negligible effect on the reaction rate for reactions that have large activation energies (under conditions similar to those in this work).[3] Stewart[14] showed that for most supercritical fluid flow applications the diffusion coefficient is of the order of 10^{-7} m^2/s. Liquids generally have a diffusion coefficient of the order 10^{-8} m^2/s. In our experiment, the fluid transitions from an initial compressed liquid state into a supercritical fluid. Therefore, the diffusion coefficient was set to a constant value of 10^{-8} m^2/s where the fluid is subcritical and 10^{-7} m^2/s where the fluid is supercritical.

Several simulations of flow through the reactor (0.5 mm i.d. and 34.3 cm in length) were performed using different grid densities $(z\times r)$: 80×15 and 200×25. A comparison of the results obtained from the two grids indicated a negligible (less than 0.5%) difference in the bulk fuel temperature and reaction rate calculations. Because the 200×25 grid runs took five times longer to execute than the 80×15 grid and resulted in a negligible accuracy gain, all subsequent solutions were calculated using the 80×15 grid.

The formation of products from cracking n–decane is calculated using a PPD mechanism.[3] The PPD mechanism is based on the observation that for mild cracking of n–alkanes each product forms at a constant proportion with respect to the other products. Therefore, it is possible to predict the mass fractions of the cracked products formed by taking advantage of these PPDs. However, in our previous work, the PPD mechanism was only validated for one pressure condition.[3] Qualifying the expansion of the PPD mechanism to a range of pressures is an objective of the present work. The product mass fraction of species i (y_i) is measured from the experimental data,

$$y_i = Y_i/Y_{\sum \text{products}} \tag{3}$$

Equation (3) represents the fraction of species i of the sum of the products (excluding the parent fuel). By the PPD assumption, y_i remains approximately constant (small variations due to experimental uncertainty) over a range of n–decane conversions. The arithmetic average of several y_i, measured from different experimental conditions (n–decane conversions), is calculated to obtain species product distributions that can be used over the range of conversions

Table 2 Arrhenius rate constants used in the CFD calculations, n-decane, $C_{12}H_{26}$

Model	E_a, k cal/mol	A, s^{-1}
Present[a]	63	1.6×10^{15}
Stewart et al.[21b]	64 ± 2.4	$1.10 \times 10^{15.9 \pm 1.5}$
Ward et al.[3c]	63	2.1×10^{15}

[a] $P = 3.45$–11.38 MPa and $T = 550$–600°C.
[b] $P = 2.96$ MPa and $T = 440$–535°C.
[c] $P = 3.45$ MPa and $T = 500$–600°C.

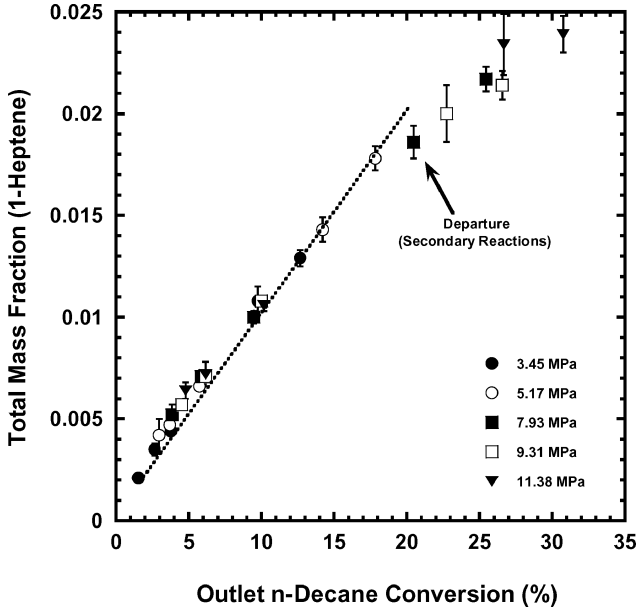

Fig. 4 Measured 1–heptene formation.

considered. In Eq. (3), Y_i is the individual product species fraction of the total fuel mixture (including the parent fuel). It can be calculated by multiplying the total product mass fraction by the average product fractions of each individual species, $y_{i_{av}}$,

$$Y_i = (1.0 - Y_{RH}) \cdot y_{i_{av}} \tag{4}$$

One rate expression is used to predict the conversion of n–decane into products [Eq. (5)]. RH denotes the concentration of the parent fuel,

$$-\frac{d(RH)}{dt} = k_A[RH] \tag{5}$$

The rate constant k_A for the reaction of Eq. (5) is expressed in the Arrhenius form:

$$k_A = A \cdot \exp(-E_a/RT) \tag{6}$$

Table 2 shows the rate constants used in the simulations.

Therefore, the PPD mechanism described in Eqs. (3–6) is capable of calculating the chemical composition of a fuel as it cracks using only one rate expression governing the degradation of the parent fuel (n–decane).

Results and Discussion

It has been observed that, for mild-cracking reactions of n–hexadecane, the first-order rate constant was independent of pressure over the ranges studied,[4] 1.38–6.89 MPa. To examine whether this observation would be true for n–decane as well, the same set of rate constants were used in simulating the measurements over every pressure, temperature, and flow rate condition. The rate constants used to predict n–decane conversion are within the error bounds of those determined from flow reactor experiments at similar experimental

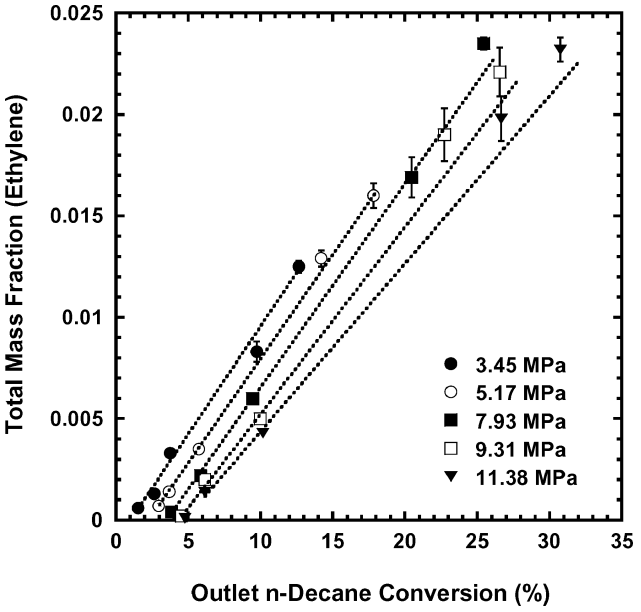

Fig. 5 Measured ethylene formation.

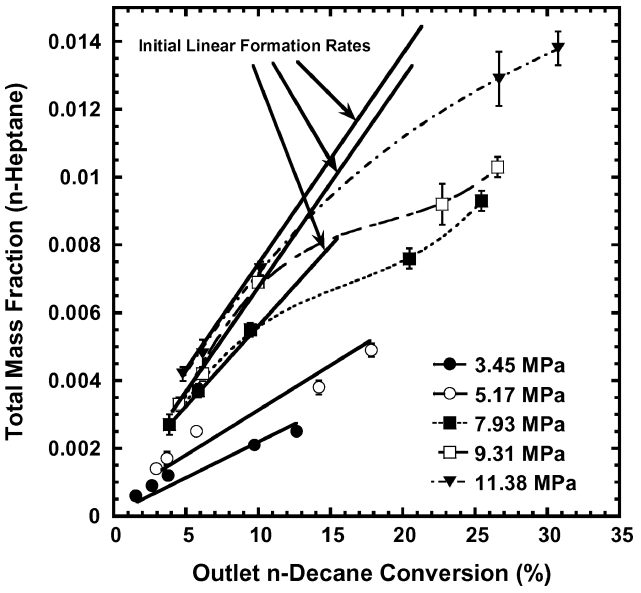

Fig. 6 Measured n–heptane formation.

conditions. Because the rate constants were used to predict conversions at different conditions than the literature values, a small variation from the mean literature values was required. Table 2 shows that the rate constants used in this work are similar to that used in our previous work.[3] (E_a is identical.) The A factor was slightly changed (but still within the error bounds of Table 2) for better agreement between the results and the experimental measurements.

The PPD mechanism has previously been defined as valid for mild-cracking conditions only. This is because significant secondary cracking of the initial products will cause the product distribution to become nonproportional.[3] Therefore, it is important to determine the percent of n–decane conversion at which secondary cracking becomes significant. Figures 4–6 show the measured formation of several selected products with increased conversion of n–decane (obtained by varying the wall temperature, flow rate, and pressure). The selected products are representative of three behavior classes of products: C_4–C_9 n–alkane products (represented by 1–heptane), C_1–C_3 products (represented by ethylene), and C_4–C_9 1–alkene products (represented by 1–heptene).

Figure 4 shows that 1–heptene initially forms at a linear rate as the conversion of n–decane increases, regardless of the pressure.

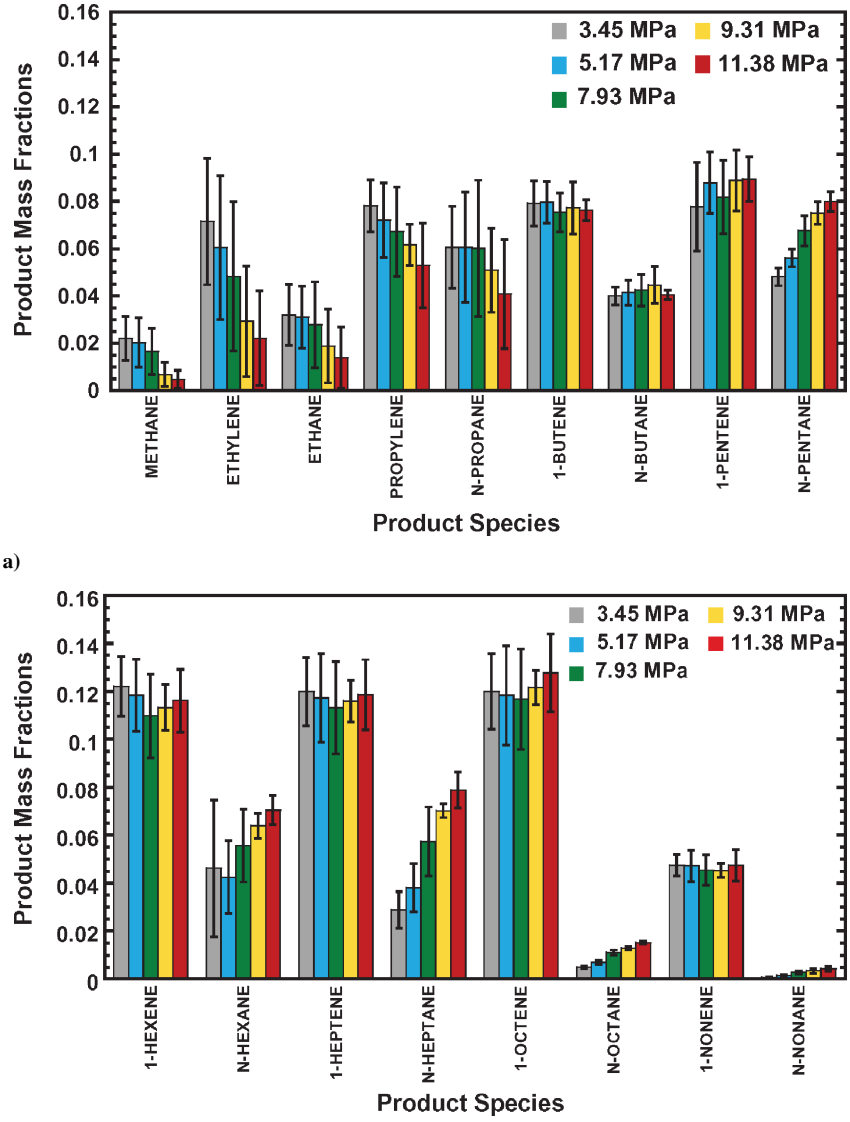

Fig. 7 PPDs for varying pressures, constant pressure PPDs: a) C_1–C_5 products and b) C_6–C_9 products.

However, at a conversion of approximately 20%, 1–heptene deviates from the initial linear formation rate. This indicates that, at conversions greater than 20%, a portion of the 1–heptene initial product is cracking into smaller secondary products. This is the same conversion where secondary cracking was first observed in previous n–decane experiments[3] at a pressure of 3.45 MPa.

Figure 5 shows that, for conversions of less than 20%, ethylene also forms at a linear rate. However, for conversions greater than 20%, the measured ethylene begins to exceed the initial linear rate. The additional ethylene is likely formed from secondary cracking of higher carbon number initial products.[3] Figure 5 shows that increasing pressure tends to decrease the amount of n–decane conversion to ethylene. The strong influence of pressure on formation rate of ethylene shown in Fig. 5 contrasts greatly with the weak influence pressure has on the formation of 1–heptene in Fig. 4.

Contrary to the linear formation rates observed in Fig. 4, the linear formation rates of ethylene in Fig. 5 do not extrapolate through the origin. This is because ethylene is primarily formed from the unimolecular decomposition of radicals resulting from the initial n–decane decomposition. At higher pressures, these radicals are more likely to react via bimolecular reactions, which do not form ethylene. Thus, the linear formation rates move away from the origin at higher pressures.

Similar to Figs. 4 and 5, Fig. 6 shows that the formation rate of n–heptane is approximately linear for n–decane conversions less than 20%. However, as the conversion of n–decane becomes greater than 20%, the formation of n–heptane decreases, indicating that it is cracking into secondary products. Figure 6 also shows that increasing pressure significantly increases the formation of n–heptane.

Figures 4–6 indicate that significant secondary cracking occurs for n–decane conversions greater than 20%. Therefore, because of the mild-cracking assumption, the PPD mechanism loses validity for simulations involving n–decane conversions greater than 20%.

Figures 7a and 7b show the PPD obtained from the measured data [Eq. (3)] for each pressure. (Product distributions measured beyond the 20% limit were not averaged into the PPD models.) The error bars represent the standard deviation of the product mass fraction over each temperature and flow rate condition for a constant pressure. Figures 4–7 indicate that as pressure increases the C_4–C_9 n–alkane products, for example, 1–heptane, form in greater proportions, whereas the smaller C_1–C_3 products, for example, ethylene, proportionally decrease, and the formation of C_4–C_9 1–alkene products, for example, 1–heptene, remains relatively constant. Previous experiments have shown similar results with increasing pressure.[4,5] In both Refs. 4 and 5, an increased pressure increased the percentage of higher molecular weight normal alkane products at the expense of lower molecular weight products. This behavior can be better understood by considering the mechanism developed by Kossiakoff and Rice,[22] which describes the decomposition of hydrocarbons through a series of free radical reactions.

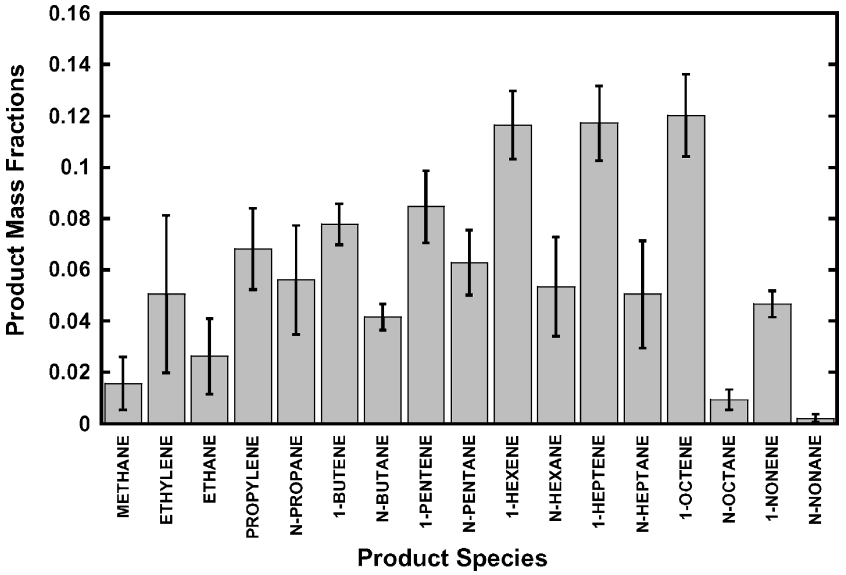

Fig. 8 Averaged PPD over all of the pressures, general PPD.

Initiation:

$$\mathrm{RH} \rightarrow R\cdot + R\cdot \tag{7}$$

Bimolecular reaction:

$$R\cdot + \mathrm{R'H} \rightarrow \mathrm{RH} + R'\cdot \tag{8}$$

Unimolecular reaction:

$$R\cdot \rightarrow R''\cdot + \text{alkene} \tag{9}$$

Equation (7) shows that decomposition initiates by a carbon–carbon bond fission along the parent n–alkane chain (RH) to form radicals ($R\cdot$). The radicals can then either react through bimolecular [Eq. (8)] or unimolecular reactions [Eq. (9)]. In a bimolecular reaction, the radicals abstract hydrogen atoms from surrounding molecules to form an n–alkane (RH) and another radical ($R'\cdot$). In a unimolecular reaction, $R\cdot$ decomposes by a β-scission reaction to form an alkene and a smaller radical ($R''\cdot$). The radicals formed can then repeat the reaction processes, shown in Eqs. (8) and (9), resulting in alkene and n–alkane products of different chain lengths. Pressure increases the molecular collision frequency, which enhances bimolecular processes more than the unimolecular processes. Thus, as pressure increases, more n–alkanes are produced relative to alkenes.

Because Figs. 7a and 7b show that the product distribution changes with pressure, one might presume the necessity of defining a different PPD model for each constant pressure. It would be more generally applicable if only one PPD could be defined over a range of pressures. Figures 7a and 7b show that the C_4–C_9 1–alkene products form in greater proportions and vary less (nearly constant) with pressure relative to the other products. This observation suggests that a general PPD model (for a range of pressures) could be constructed by averaging the measured product fractions over the entire pressure range studied in the experiment, 3.45–11.38 MPa. The primary source of error of this general PPD model will be caused by averaging over the pressure-varying C_4–C_9 n–alkane and C_1–C_3 products. It is worth exploring if this error is acceptably small enough to provide a general PPD model that reasonably represents the behavior observed in the current experiments.

Figure 8 shows a new general PPD obtained by averaging all five of the constant pressure product distributions shown in Figs. 7a and 7b. Because ethylene experiences the greatest relative change over the range of pressures used in the experiment (Fig. 7a), it can be used to estimate the maximum error that this general PPD model

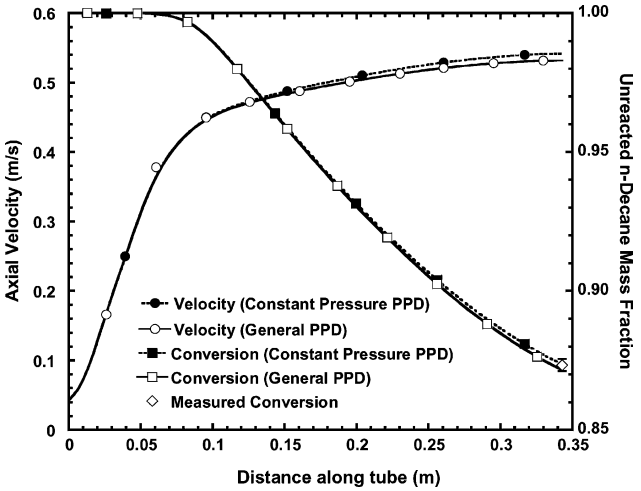

Fig. 9 Flow property calculation comparison between a constant pressure, 3.45 MPa, PPD and a general PPD mechanism.

(Fig. 8) will have in predicting a single product. Previous pyrolysis experiments also showed that ethylene underwent the largest product formation change with varying pressure.[5] A comparison of the ethylene distribution in Fig. 7a (for both pressure extremes of 3.45 and 11.38 MPa) to the averaged ethylene distribution in Fig. 8 shows a maximum difference of 42%. Although this difference would be significant in isolation, it represents a difference of only 2.1% relative to the total product mixture. Also, the averaged ethylene distribution (Fig. 8) lies within the error bars of the measured ethylene for every pressure condition (Fig. 7a), with just one exception. (The upper error bar for 11.38 MPa in Fig. 7a falls just 0.005 under the average distribution.) Therefore, the general PPD model may be worth further investigation.

The maximum species mass fraction difference between any of the constant pressure PPDs (Fig. 7) and the general PPD (Fig. 8) occurs at 3.45 MPa. Figure 9 shows a comparison between the calculated axial velocities and n–decane mass fractions using the constant pressure (3.45 MPa) and general PPD models. The intent of Fig. 9 is to show the difference in the results obtained by using the general PPD model compared to the constant pressure PPD model. The axial velocity and n–decane mass fraction were selected for Fig. 9 because they are good indicators of differences in the flow property and cracking reaction results, respectively. The

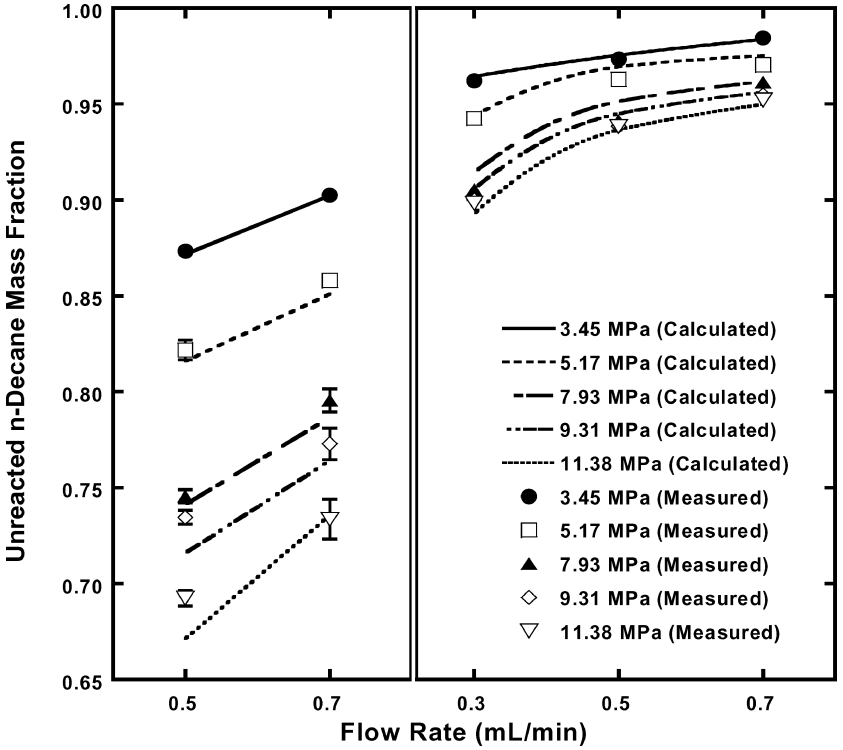

Fig. 10 Comparison of measured and simulated (general PPD) outlet unreacted n–decane mass fraction, maximum wall temperature a) 600°C and b) 550°C.

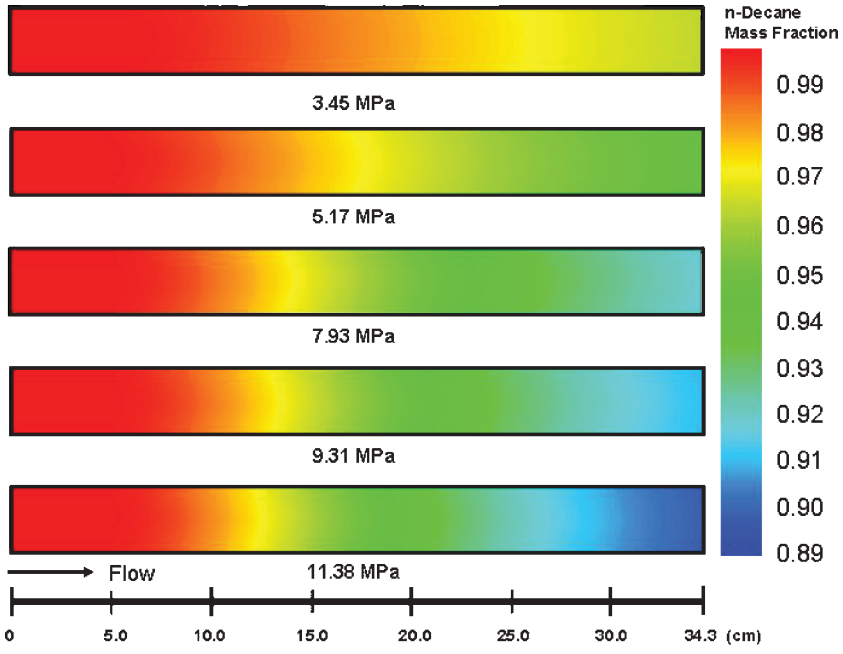

Fig. 11 Pressure effects on calculated n–decane mass fraction, two-dimensional plot.

experimental conditions (maximum wall temperature of 600°C and flow rate of 0.5 ml/min) of Fig. 9 correspond to maximum conversion at 3.45 MPa. Figure 9 shows that both n–decane conversion calculations agree closely (within the error bounds) of the measured outlet n–decane conversion. The maximum difference between the two predicted n–decane conversions is less than 0.25% conversion. The axial velocity calculations also agree reasonably well with a maximum difference of 1.8%. Because the n–decane conversion and velocity calculations do not vary appreciably using the general PPD relative to the constant pressure PPD, we conclude that the error associated with the general PPD is within an acceptable tolerance, for our purposes, over the range of pressures studied. The general PPD model will now be used to study the behavior of pyrolytic fuel flow at varying pressures.

Figure 10 shows a comparison of the measured outlet n–decane conversion to the simulated results (general PPD model). Figure 10 shows that, as pressure increases, the conversion of n–decane also increases. The simulation agrees with the measured values within approximately ±1% (conversion), at conversions less than 20% (within the PPD mechanism accuracy limit). At conversions greater

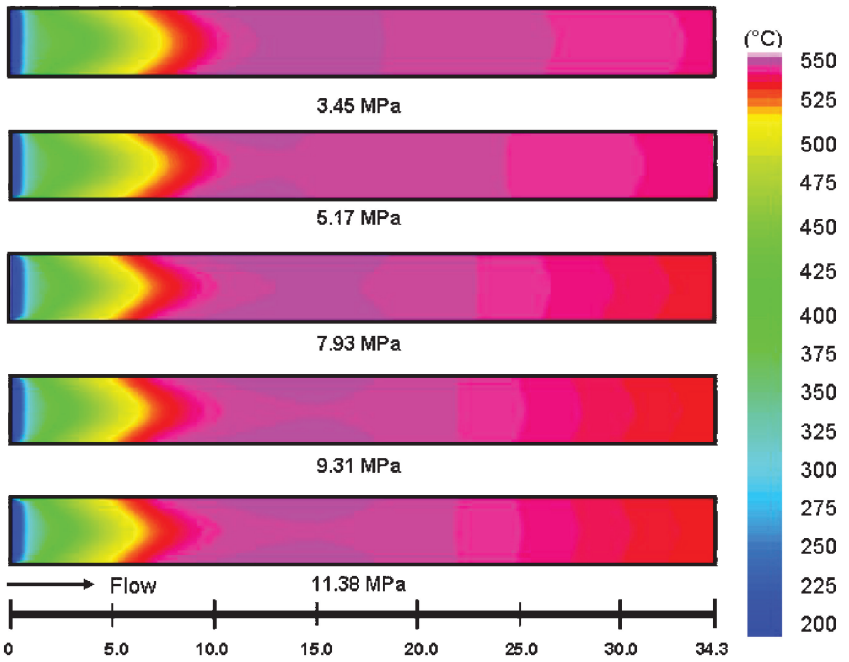

Fig. 12 Pressure effects on calculated fuel temperature, two-dimensional plot.

than 20%, the differences between calculated and measured values gradually increases as the conversion increases, possibly due to increased formations of products from secondary reactions.[3] Figure 10 also shows that the effect of increased n–decane conversion with pressure is primarily due to factors other than a change in the rate constant. Because k_A was held constant in Eq. (5), the change in conversion rate must primarily be influenced by changes in the flow properties with pressure. A closer examination of the computed flow properties can assist in understanding the effect of pressure on conversion.

Figure 11 shows the calculated mass fraction of n–decane as it flows through the reactor at different pressures but at the same maximum wall temperature, 550°C, and flow rate, 0.3 ml/min. These conditions were selected because they yield the maximum conversion in the experiment, while still below the PPD conversion limitation for every pressure (Fig. 10). Because the same rate constants and input conditions (wall temperature and flow rate) were used for every simulation in Fig. 11, the change in the reaction rate is only due to the effects of pressure. Figure 11 shows that varying pressure does not significantly affect the radial mass fraction profile but dramatically affects the axial profile.

Figure 12 shows calculated fuel temperature as it flows through the reactor at the same conditions as Fig. 11. In both the experiment and the simulation, a constant wall temperature profile was input, regardless of pressure or flow rate. In the experiment, the heating source was adjusted to attain the same maximum wall temperature (550 or 600°C). Because the wall temperature and flow rate are held constant, the fuel temperature will only vary due to pressure induced effects.

Figure 12 shows that the fuel temperature reaches its peak and levels off at approximately 10 cm along the reactor for each pressure condition. However, as pressure increases, resulting in an increase in n–decane conversion (Fig. 11), the fuel cools more due to the higher endotherm generated by the pyrolytic reactions.

Several flow properties were examined (at the same conditions as Figs. 11 and 12, maximum wall temperature of 550° and flow rate of 0.3 ml/min) to determine which properties are most affected by pressure and their influence on the decomposition of n–decane. Figures 13–16 show the change in the bulk fuel temperature and several bulk flow properties as pressure varies. The bulk values are calculated by averaging properties at each grid point across the radial length of the reactor.

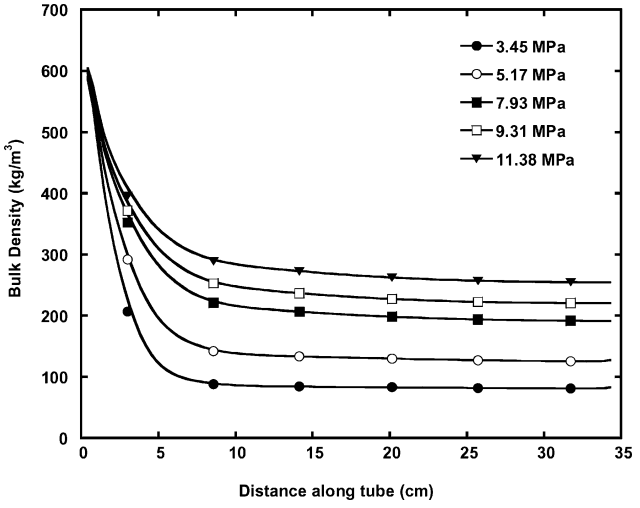

Fig. 13 Pressure effects on calculated bulk density.

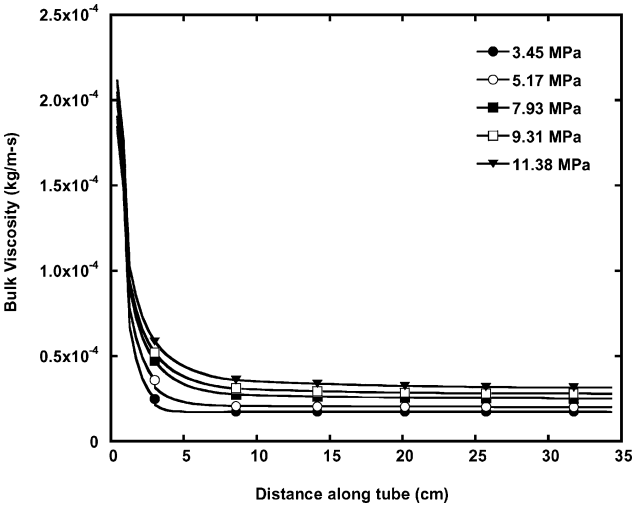

Fig. 14 Pressure effects on calculated bulk viscosity.

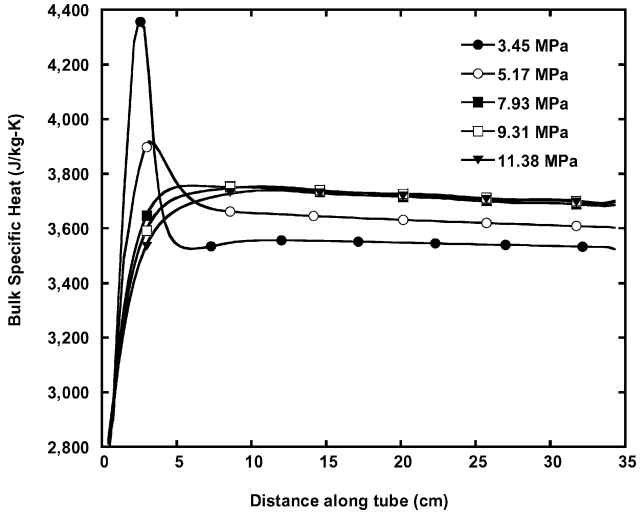

Fig. 15 Pressure effects on calculated bulk specific heat.

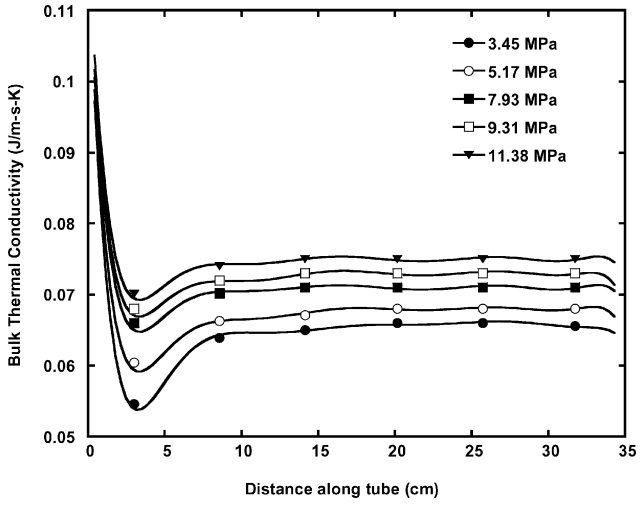

Fig. 16 Pressure effects on calculated bulk thermal conductivity.

Figure 13 shows that the bulk density is significantly affected by pressure changes. When only the portion of the tube after 10 cm is considered, density increases by about 200%, as pressure increases from 3.45 to 11.38 MPa. Figure 17 shows the calculated dimensionless density of the fuel and demonstrates that increasing pressure inhibits reduction of the fuel density within the reactor. By conservation of mass, as density increases, the velocity will decrease. Because velocity is proportional to residence time (which directly affects the extent of conversion), an increased density increases the conversion rate. However, conversion of n–decane into lighter cracked products also decreases the density. Density and the chemical decomposition of the reaction mixture are closely coupled.

Figure 14 shows (after 10 cm along the reactor) that the bulk viscosity increases by 60% over the range of pressures studied. An increased viscosity increases the residence time and, therefore, the heat transfer rate of flow near the walls. This observation justifies the use of a two-dimensional simulation. (A plug flow simulation is not capable of simulating property changes in the radial direction.)

At the critical point, the specific heat diverges and approaches infinity. In the vicinity of the critical point, the specific heat can be much larger than its subcritical or supercritical value. In Fig. 15 the specific heat for the pressure of 3.45 MPa initially rises and peaks at 3 cm along the reactor, which corresponds to the fuel's closest approach to the critical point, for n–decane $P_c = 2.10$ MPa and $T_c = 345°$C. At this point, there is a 20% difference between the specific heat (for 3.45 MPa) and the specific heats corresponding to the higher pressures (7.93, 9.31, and 11.38 MPa). The specific heat (for 3.45 MPa) then declines as the fuel transitions from a compressed liquid to a supercritical fluid. After 10 cm along the tube, the difference between all of the specific heats (over the entire range of pressures) declines to only 7%. The specific heat (for 5.17 MPa) also peaks (at approximately the same point along the reactor) but below the specific heat peak (for 3.45 MPa). As pressures increases and moves away from the critical point (7.93, 9.31, and 11.38 MPa), the peaks disappear.

Figure 16 shows the variation of thermal conductivity along the reactor. At the critical point, the thermal conductivity approaches zero. In the vicinity of the critical point, the thermal conductivity can be much smaller than its subcritical or supercritical values. Figure 10e shows that the thermal conductivity declines and reaches a minimum point at 3 cm along the reactor (closest approach to the critical point). At these minima, there is a 20% difference in the thermal conductivities over the range of pressures. However, after

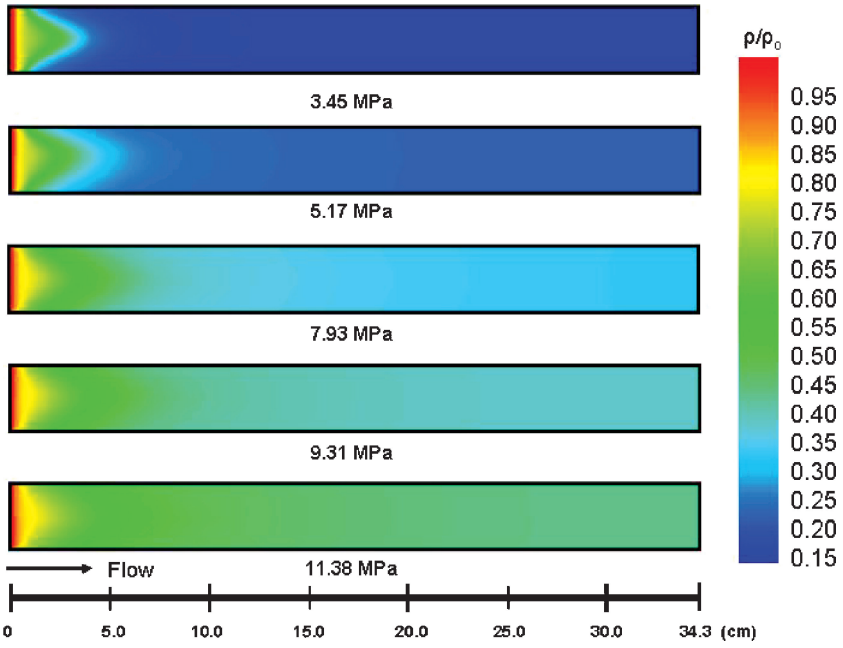

Fig. 17 Pressure effects on calculated fuel density, two-dimensional plot. (Maximum Wall Temperature: 550°C, Flow Rate: 0.3 mL/min).

10 cm along the tube, the bulk thermal conductivity changes by only 7% over the range of pressures. Figures 15 and 16 illustrate the importance of incorporating SUPERTRAPP into the CFD model to simulate accurately the flow properties near the critical point and in the supercritical region.

The effect of pressure on the endothermic heat sink (at the same conditions as Figs. 11–17) is shown in Fig. 18. The change in enthalpy of the fuel due only to the endothermic chemical reactions, Δh_{endo}, was calculated by

$$\Delta h_{endo} = h_{tot} - h_{sens} \tag{10}$$

In Eq. (10), enthalpy changes due only to sensible heat transfer h_{sens} are subtracted from the total enthalpy h_{tot}. The sensible enthalpy h_{sens} was obtained by running the CFD simulation without the cracking chemistry. The total enthalpy h_{tot} was obtained by running the simulation with the PPD chemistry mechanism and, therefore, includes the effects of both sensible heat transfer and the endothermic chemical reactions.

Figure 18 shows that as pressure increases the endothermic heat sink increases. The cracked products have a higher enthalpy than the n–decane parent fuel. As more products form, the overall enthalpy of the fuel mixture increases. Because increasing pressure increases the amount of cracked products formed (Fig. 10), increasing pressure also increases the endothermic heat sink. Figure 18 also shows that each of the Δh_{endo} curves peak before the end of the reactor. This is because the fuel cools as a result of the endothermic heat sink, which in turn cools the reactor wall. This can be seen in Fig. 3. As the wall cools, the heat transfer rate into the fuel declines, and therefore, the enthalpy decreases.

Figure 18 also shows a small peak in the heat sink curves near the beginning of the reactor (before 10 cm). This peak is not due to an endotherm, but is most likely just an anomaly caused by proximity of the fuel properties to the critical point. Near the beginning of the reactor, only a very small amount of fuel (near the wall) is cracked. Therefore, in this region, there should be very little difference between the flow properties of the reacting and nonreacting fuel flow simulations and the calculated endothermic heat sink should essentially be zero [Eq. (10)]. However, near the critical point, small differences in the flow properties can have a large effect on the enthalpy of the fuel. The variations of the two enthalpies in Eq. (10) (which each have slightly different flow properties due to the PPD mechanism being on or off) near the critical point are the most likely cause of the anomaly. As the flow properties of the fuel move away from the critical point, this anomaly vanishes (after 10 cm along the tube).

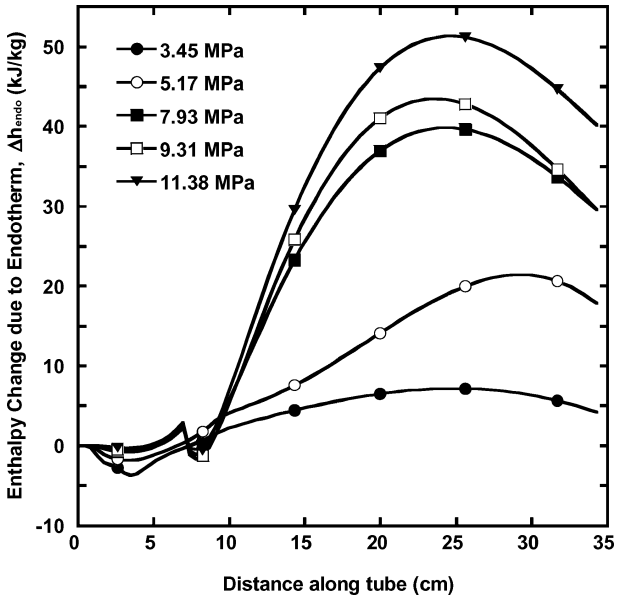

Fig. 18 Pressure effects on the calculated endothermic heat sink.

Table 3 Calculated heat transfer rates[a]

Pressure, MPa	Q_{tot}, W	Q_{sens},[b] W	Q_{endo},[c] W
3.45	3.578	4.907	− 1.329
5.17	3.566	4.941	− 1.375
7.93	3.563	4.990	− 1.427
9.31	3.544	5.012	− 1.468
11.38	3.567	5.043	− 1.477

[a]Maximum wall temperature = 550°C and flow rate = 0.3 ml/min.
[b]No reactions.
[c]$Q_{tot} - Q_{sens}$.

Table 3 shows calculated heat transfer rates of the simulations shown in Fig. 18. The calculations were done using a first-law analysis of the entire tube under conditions of steady flow. Bulk properties were used to simplify the calculation. The total endothermic heat transfer rate Q_{endo} was obtained by

$$Q_{endo} = Q_{tot} - Q_{sens} \tag{11}$$

Equation (11) is similar to Eq. (10). The sensible heat transfer Q_{sens} was calculated by using flow properties obtained from running the CFD simulation with the cracking chemistry mechanism disengaged. The total heat transfer Q_{tot} was calculated by using flow properties obtained from running the simulation with the PPD chemistry mechanism engaged and, therefore, includes the effects of both sensible heat transfer and the endothermic chemical reactions.

Table 3 shows that sensible heat transfer Q_{sens} is higher than the total heat transfer Q_{tot}. This is because the endothermic cracking reactions cool the fuel. Because the reactor wall is heated by the furnace at a constant rate, there is no additional heat to balance the cooling from the fuel as it reacts, and so the reactor wall cools. Table 3 shows that, as pressure increases, the total endotherm Q_{endo} also increases due to increased cracked products (Fig. 10). In this experiment, the magnitude of Q_{endo} is relatively small because the diameter of the reactor is very small, 0.5 mm i.d. Larger diameter tubes would have the potential to yield significantly higher endotherms.

Pressure affects both the reaction rates and the flow properties. The interaction among the properties is complex and coupled. All of the flow properties examined in Figs. 13–16 were affected by pressure and influenced the fuel's chemical kinetics. Density appears to be the most significant property because it increased by 200% over the 3.45–11.38 MPa pressure range. Viscosity is also significant because it increased by 60% over the pressure range. The specific heat and thermal conductivity were least significant because both increased by only 7% over the pressure range. The coupling of the chemical kinetics and flow properties illustrates the importance of simulating their complex interactions in a multidimensional CFD model. The observation that increasing pressure influences the conversion rate of the fuel implies possible applications to an endothermic heat exchanger system. Backpressure valves could potentially be used to throttle the pressure to attain a desired conversion rate and endotherm. These valves could potentially be controlled via a feedback loop to ensure that the fuel does not surpass mild-cracking limitations to ensure minimum surface deposition. It is believed that a multidimensional CFD simulation, using the techniques presented in this work, could be an invaluable tool in the design of future endothermic fuel systems.

Conclusions

The use of endothermic fuels is a promising alternative to meet the growing high-heat-sink requirements of future high-performance aircraft. However, little work has been done to analyze the effects of pressure on a chemically reacting, flowing fuel. The experiments performed in this work show that increasing pressure enhances the processes in which n–decane converts to (C_5–C_9) n–alkane products instead of decomposing into lower molecular weight products (C_1–C_4). A two-dimensional CFD model was developed that predicts the formation of pyrolysis products by using experimentally derived PPDs. It was shown that a general PPD mechanism could

be defined to simulate fuel pyrolysis over a range of pressures, temperatures, and flow rates. The model was used to simulate the effect of pressure on the complex coupling of the mass and transport properties involved with supercritical chemically reacting fuels. It was shown that increasing pressure increases the overall conversion rate (and, therefore, the endotherm) of flowing, supercritical n–decane. This is primarily because pressure increases the density, which decreases the residence time of n–decane flowing through the reactor. It is anticipated that this model could serve as a building block to computational models involving more complex endothermic fuels and cooling systems.

Acknowledgments

This work was supported by the U.S. Air Force National Aerospace Fuels Research Complex (AFRL/PRTG) at Wright–Patterson Air Force Base, Ohio; the University of Dayton Research Institute (under Contract F33615-03-2-2347); and the Dayton Area Graduate Studies Institute.

References

[1]Sobel, D. L., and Spadaccini, L. J., "Hydrocarbon Fuel Cooling Technologies for Advanced Propulsion," *Journal of Engineering for Gas Turbines and Power*, Vol. 119, No. 2, 1997, pp. 344–351.

[2]Heinrich, B., Luc-Bouhali, A., Ser, F., and Vigot, C., "Endothermic Liquid Fuels: Some Chemical Considerations on the Cooling Process," AIAA Paper 2001-1785, April 2001.

[3]Ward, T. A., Ervin, J. S., Striebich, R. C., and Zabarnick, S., "Simulations of Flowing Mildly Cracked Normal Alkanes Incorporating Proportional Product Distributions," *Journal of Propulsion and Power*, Vol. 20, No. 3, 2004, pp. 394–402.

[4]Fabuss, B. M., Smith, J. O., Lait, R. I., Borsanyi, A. S., and Satterfield, C. N., "Rapid Thermal Cracking of n-Hexadecane at Elevated Pressures," *Industrial and Engineering Chemistry Process Design and Development*, Vol. 1, 1962, pp. 293–299.

[5]Jones, G. E., Balster, L. M., and Balster, W. J., "Effect of Pressure on Supercritical Pyrolysis of n-Paraffins," *Proceedings of the Symposium on General Papers Division of Petroleum Chemistry*, American Chemical Society, 1999, pp. 394–397.

[6]De Witt, M. J., and Broadbelt, L. J., "Binary Interactions between Tetradecane and 4- (1-Napthylmethyl) Bibenzyl During Low- and High Pressure Pyrolysis," *Energy and Fuels*, Vol. 13, 1999, pp. 969–983.

[7]Nigam, A., and Klein, M. T., "A Mechanism-Oriented Lumping Strategy for Heavy Hydrocarbon Pyrolysis: Imposition of Quantitative Structure-Reactivity Relationships for Pure Components," *Industrial and Engineering Chemistry Research*, Vol. 32, 1993, pp. 1297–1303.

[8]Ranzi, E., Dente, M., Pierucci, S., and Biardi, G., "Initial Product Distributions from Pyrolysis of Normal and Branched Paraffins," *Industrial and Engineering Chemistry Fundamentals*, Vol. 22, 1983, pp. 132–139.

[9]Bozzano, G., Dente, M., Faravelli, T., and Ranzi, E., "Fouling Phenomena in Pyrolysis and Combustion Process," *Applied Thermal Engineering*, Vol. 22, 2002, pp. 919–927.

[10]Ervin, J. S., Ward, T. A., Williams, T. F., and Bento, J., "Surface Deposition within Treated and Untreated Stainless-Steel Reactors Resulting from Thermal-Oxidative and Pyrolytic Degradation of Jet Fuel," *Energy and Fuels*, Vol. 17, No. 3, 2003, pp. 577–586.

[11]Lindstedt, R. P., and Maurice, L. Q., "Detailed Chemical-Kinetic Model for Aviation Fuels," *Journal of Propulsion and Power*, Vol. 16, 2000, pp. 187–195.

[12]Liguras, D. K., and Allen, D. T., "Comparision of Lumped and Molecular Modeling of Hydropyrolysis," *Industrial and Engineering Chemistry Research*, Vol. 31, 1992, pp. 45–53.

[13]LinhBao, T., and Chen, L. D., "Heat Transfer Calculation of an Endothermic Fuel at Supercritical Conditions," AIAA Paper 98-3762, July 1998.

[14]Stewart, J. F., "Supercritical Pyrolysis of the Endothermic Fuels Methylcyclohexane, Decalin, and Tetralin," Ph.D. Dissertation, Princeton Univ., Princeton, NJ, June 1999.

[15]Goel, P., and Boehman, A. L., "Numerical Simulation of Jet Fuel Degradation in Flow Reactors," *Energy and Fuels*, Vol. 14, 2000, pp. 953–962.

[16]Huang, H., Sobel, D. R., and Spadaccini, L. J., "Endothermic Heat-Sink of Hydrocarbon Fuels for Scramjet Cooling," AIAA Paper 2002-3871, July 2002.

[17]Patankar, V. S., *Numerical Heat Transfer and Fluid Flow*, McGraw–Hill, New York, 1980.

[18]Launder, B. E., and Spalding, D. B., "The Numerical Computation of Turbulent Flows," *Computer Methods in Applied Mechanics and Engineering*, Vol. 3, 1974, pp. 269–289.

[19]Ely, J. F., and Huber, M. L., *NIST Standard Reference Database 4—NIST Thermophysical Properties of Hydrocarbon Mixtures*, Ver. 3.0, National Inst. of Standards and Technology, Gaithersburgh, MD, Oct. 1999.

[20]Peng, D., and Robinson, D. B., "A New Two-Constant Equation of State," *Industrial and Engineering Chemistry Fundamentals*, Vol. 15, 1976, pp. 59–64.

[21]Stewart, J., Brezinsky, K., and Glassman, I., "Supercritical Pyrolysis of Decalin, Tetralin, and N-Decane at 700-800 K. Product Distribution and Reaction Mechanism," *Combustion Science and Technology*, Vol. 136, 1998, pp. 373–390.

[22]Kossiakoff, A., and Rice, F. O., "Thermal Decomposition of Hydrocarbons, Resonance Stabilization and Isomerization of Free Radicals," *Journal of the American Chemical Society*, Vol. 65, 1943, pp. 590–595.